Chemical Geology 324–325 (2012) 122–131

Contents lists available at SciVerse ScienceDirect

Chemical Geology

journal homepage: www.elsevier.com/locate/chemgeo

Research paper

The quantification and application of handheld energy-dispersive x-ray fluorescence (ED-XRF) in mudrock chemostratigraphy and geochemistry

Harry Rowe, Niki Hughes *, Krystin Robinson

Earth and Environmental Sciences, University of Texas at Arlington, 500 Yates Street, Arlington, TX, USA

ARTICLE INFO

Article history:
Accepted 20 December 2011
Available online 8 January 2012

Editor: J.D. Blum

Keywords:
Major and trace elements
Calibration
Shale
Mudstone

ABSTRACT

Traditionally, analytical techniques such as wavelength-dispersive x-ray fluorescence (WD-XRF), inductively-coupled plasma (ICP) and mass spectrometry (ICP-MS), instrumental neutron activation analysis (INAA), or stationary (bench-top) energy-dispersive x-ray fluorescence (ED-XRF) have been used to generate quantitative geochemical results. However, a more efficient means of data collection using portable ED-XRF instrumentation now allows the investigator to acquire rapid, non-destructive, quantitative measurements on drill core and clean, flat rock surfaces, in addition to pressed powder pellets typically used in WD-XRF analysis. Similar to traditional XRF methods, quantification using the handheld ED-XRF requires a matrix-specific calibration. Unfortunately, very few internationally-accepted mudrock or shale reference materials exist, and their elemental ranges provide inadequate coverage for the geochemical diversity of mudrocks. In order to return reliable, calibrated results, a unique set of reference materials has been developed that incorporates a wide range of mudrock elemental compositions. The current method provides elemental calibrations for major elements heavier than sodium, and the following trace elements: Ba, V, Cr, Ni, Cu, Zn, Rb, Sr, Y, Zr, Nb, Mo, Th, and U.

A comparison of handheld energy-dispersive and wavelength-dispersive x-ray fluorescence (ED-XRF and WD-XRF) results from pressed powder pellets of Mississippian-age Barnett Shale of North-Central Texas, USA, is presented in order to evaluate the reliability of the reference calibration and the quantification of unknown samples using two different instrument platforms. It will be demonstrated that calibrated results from the handheld ED-XRF effectively define chemostratigraphic changes in real-time. As a consequence, quantified results can be used immediately to assess changes in bulk mineralogy, paleo-redox conditions, and to link down-core geochemical changes to stratigraphic, sedimentological, and paleoenvironmental observations.

1. Introduction

While the x-ray fluorescence technique has been used to generate quantitative geochemical results for many decades (Norrish and Hutton, 1969; Potts and Webb, 1992; Tertian and Claisse, 1994; Fitton, 1997), major advances in the utilization of x-ray fluorescence to address stratigraphic shifts in the chemistry of sediments and rocks have occurred in recent years (e.g., Jansen et al., 1999; Haug et al., 2001; Rimmer, 2004; Richter et al., 2006; Tjallingii et al., 2007; Algeo and Maynard, 2008; Kujau et al., 2010). Traditionally, it has been understood that energy-dispersive x-ray fluorescence (ED-XRF) techniques possess notably higher detection limits and lower energy resolution than typical wavelength-dispersive (WD-XRF) techniques (Fitton, 1997). While this may still be true of trace metal analyses, it is not the case for many of the major elements. Furthermore, while ED-XRF has been a useful geochemical technique for several decades, modern advances in the thin window detector, miniaturization and stability of the x-ray tube, optimization of spot-size and collimator, engineering of stable digital pulse processing circuitry, and software development have created the ability for lower detection limits, instrument portability, and novel approaches to fundamental parameters. The purpose of this study is to demonstrate the method development, its fidelity with respect to traditional WD-XRF methods, and applications of the handheld ED-XRF as a research-grade tool for analyzing mudrock geochemistry.

2. Materials and method

A mudrock suite consisting of five internationally-accepted, commercially available standards and eighty-five in-house reference materials was assembled (Table 1). The in-house reference materials were developed over several years by selecting a range of samples from diverse mudrock sequences, including the Ohio Shale of Kentucky, and the Woodford, Barnett, Smithwick, and Eagle Ford Formations of Texas, USA. All reference materials were recovered from clean drill core, powdered to 200-mesh using a low trace element, hardened-steel pulverizer, and analyzed for major and trace element composition by SGS Mineral Services, Canada. Major element concentrations were

* Corresponding author at: Encana Oil & Gas (USA) Inc., 14001 N. Dallas Pkwy, Ste. 1100, Dallas, TX 75240, USA.
E-mail address: hrowe@uta.edu (N. Hughes).

0009-2541/$ – see front matter © 2012 Elsevier B.V. All rights reserved.
doi:10.1016/j.chemgeo.2011.12.023

Table 1
Tally of minimum and maximum elemental concentrations for the suite of calibration standards and in-house reference materials.

Standards and reference materials												
	Standards[a]		Woodford Fm.[b]		Ohio Shale[c]		Barnett Fm.[d]		Smithwick Fm.[e]		Eagle Ford Fm.[f]	
n[g]	5		27		7		16		20		15	
Element	Range of values for each formation											
	Min[h]	Max[h]	Min	Max	Min	Max	Min	Max	Min	Max	Min	Max
Mg (%)	0.93	4.89	0.27	**10.25**	0.66	1.08	0.52	2.64	0.63	1.88	**0.24**	0.66
Al (%)	3.45	9.96	**0.64**	7.62	6.87	10.77	1.20	8.47	1.00	**13.07**	1.07	5.98
Si (%)	13.2	29.3	5.89	**38.2**	26.8	28.8	6.22	32.7	8.79	34.8	**3.75**	22.6
P (%)	0.02	0.14	**0.01**	0.48	0.02	0.17	0.07	**0.98**	0.03	0.12	0.02	0.15
S (%)	0.01	5.35	0.46	5.32	0.72	2.25	0.25	2.24	0.02	2.00	0.33	3.81
K (%)	1.15	3.45	0.17	3.51	2.92	**4.32**	0.27	1.83	0.22	3.12	**0.14**	1.61
Ca (%)	0.43	5.99	**0.07**	18.1	0.19	0.71	2.77	31.2	0.32	27.7	9.36	**34.7**
Ti (%)	0.16	0.43	**0.04**	0.33	0.40	0.53	0.07	0.46	0.05	**0.53**	0.04	0.39
Mn (%)	0.015	0.046	**0.008**	**0.325**	0.008	0.031	0.008	0.031	0.008	0.147	0.008	0.023
Fe (%)	2.12	**6.53**	0.61	4.92	3.09	4.60	0.64	3.54	1.66	6.38	**0.43**	3.57
Ba (ppm)	290	820	842	5750	434.3	562	63.5	625	357	**9050**	**30.3**	295
V (ppm)	87	160	51	**1720**	141	385.5	**22**	165	24	196	41	899
Cr (ppm)	30	123	20	260	62	96	40	**295**	40	120	**10**	100
Ni (ppm)	27	122	17	**302**	33.5	136.8	26	168	22	144	**11**	155
Cu (ppm)	28.7	66	8	**485**	22.3	60.5	12	83.5	8	54	**5**	66
Zn (ppm)	55	103	24	**1220**	77.1	505.3	57	387	45	301	**20**	503
Th (ppm)	4.8	12.8	**1.3**	10.7	9.1	14	2	12.9	2.1	**14.6**	1.6	9.9
Rb (ppm)	59	205	13.9	200	140.8	**224.1**	16.5	121	15.3	167	**6.4**	91.7
U (ppm)	1.5	48.8	3.36	**66**	7.2	37.3	**1.22**	11.4	1.81	6.62	1.67	14
Sr (ppm)	54	420	**36.4**	483	105.3	145	248	**869**	107	518	329	791
Y (ppm)	13	40.6	**5.8**	52.7	26.2	37.2	10.9	**62**	20	35.3	7.6	22.3
Zr (ppm)	53	165	**15.5**	122	133.9	217.7	25	146	17.2	**338**	32.6	215
Nb (ppm)	5.2	14.3	**2**	13	14	16	2	15	2	15	3	**22**
Mo (ppm)	1.4	134	9	**166**	**1.3**	153.7	2	13	2	3	3	95
Total min/max[i]	0	1	10	9	1	2	2	4	0	5	10	2

[a] International standards are SARM-41, SDO-1, Sco-1, SGR-1, and GBW-07107.
[b] Woodford Formation reference materials obtained from Reliance Triple Crown #1 core, Pecos County, TX.
[c] Ohio Shale reference materials obtained from core D4, Powell County, KY.
[d] Barnett Formation reference materials obtained from 1-Blakely core, Wise County, Texas.
[e] Smithwick Formation references obtained from Walker D-1-1 core, San Saba County, Texas.
[f] Eagle Ford Formation reference materials obtained from Leppard core, Bee County, Texas.
[g] "n" is the number of references from each unit.
[h] Minimum and maximum elemental concentrations for the entire suite are designated by bolded and underlined bolded, respectively.
[i] The total number of minimum and maximum elemental concentrations for each group of references is tallied at the bottom of the table.

determined by WD-XRF analysis of a lithium borate-fused disk (SGS method XRF76Z), and trace element concentrations were determined by ICP-MS and ICP-OES after sodium peroxide fusion and dissolution in nitric acid (SGS method ICM90A). Published concentrations for the international standards were used (Govindaraju, 1994). Sulfur concentrations for references were determined using LECO combustion/infrared analysis at the Kentucky Geological Survey. A preliminary suite of Ohio Shale reference materials was cross-checked using the XRF at the University of Cincinnati. Aliquots (~9 g) of the international standards and in-house references, backed with boric acid, were pressed to 40 tons using a 40-mm die set and an automated Carver press at the Kentucky Geological Survey.

All analyses were undertaken by laying the reference pellets on top of the instrument, which sits in a stand, with the beam pointing upward. The same is routinely done with the slabbed face of drill core, carefully balancing it on the nose of the instrument. It is critical that the sample lay directly on the instrument, as the x-ray signal would otherwise be attenuated. Each pressed pellet was analyzed in triplicate at low-energy (for major elements, plus Ba, V and Cr) and high-energy (for trace elements) conditions using a Bruker AXS TRACER III-V ED-XRF equipped with a Rh x-ray tube. Low-energy analysis was undertaken at 15 kV and 34.4 μA, under vacuum, and a count time of 360 s. High-energy analysis was undertaken at 40 kV and 25 μA, with an Al–Ti–Cu filter, and a count time of 360 s. While the voltage setting should remain constant, the current setting varies slightly between instruments, and thus, should be optimized prior to analysis and calibration. The beam size integrates a 3×4 mm area. Between measurements, each pellet was moved slightly, in order to develop a sense of reference reproducibility and uniformity of each pellet. In all, spectra from 270 analyses (90 references×3) were integrated into the major element calibration routines, and the same was done for the trace element calibration routine.

In general, for the instrument used in the present study, the signals for the low-energy spectra should be less than 13,000 raw counts/s (rcps), and for the high energy spectra should be approximately 1400 to 2000 rcps. Typical low- and high-energy spectra are shown in Fig. 1A and B. Spectra were loaded into proprietary Bruker AXS calibration software (*S1CalProcess*) within which the reference concentration of each element is evaluated against the concentration of the element as calculated using inter-element slope- and baseline-corrected peak heights from the ED-XRF system. Because the software is proprietary, a full disclosure and discussion of the calibration routine is not possible. In most instances, standards were not omitted from the calibration unless 1) reference values were below the limit of detection (as is the case for the majority of the 70 omitted values for the Mo calibration), or 2) reference values possessed studentized residuals greater than 3σ. A complete list of corrections used for the calibrations is provided (Table 2).

3. Theory: Diverse mudrock matrices improve calibration applicability

Matrix effects significantly impact sample analysis by ED-XRF and WD-XRF. And, while standardization using lab-created mixtures may be useful in some instances (e.g., Tung, 2004), obtaining a broad range of elemental concentrations and sub-matrices in the large suite of reference materials may be best accomplished by selecting

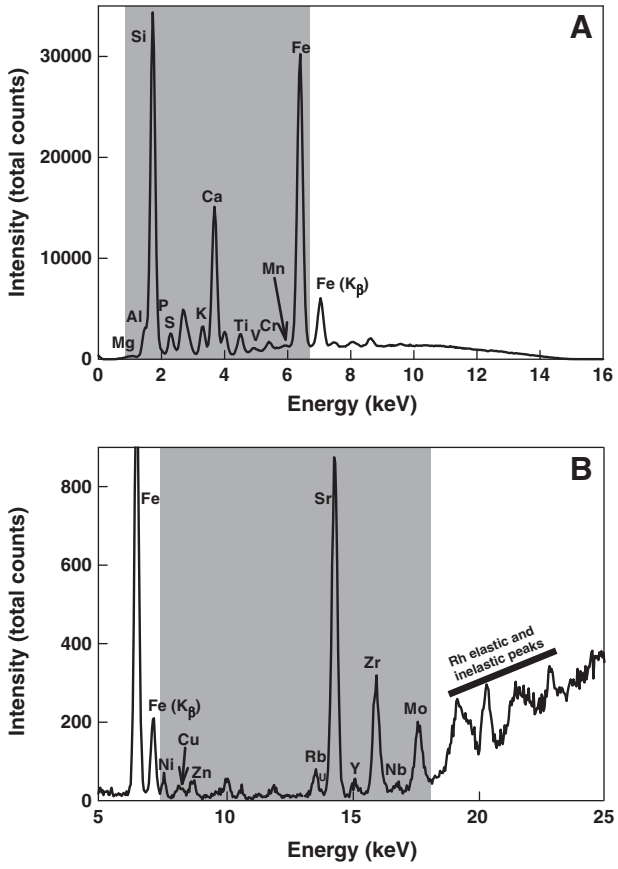

Fig. 1. A) A low-energy spectrum of a typical low-calcium sample of Barnett Shale. B) A high-energy spectrum of a typical calcium-rich sample of Eagle Ford Shale, demonstrating strong molybdenum enrichment. Spectra were generated by analyzing a pulverized, pressed sample for 3 min using low-energy (15 kV, 34.4 μA) and high-energy (40 kV, 26 μA) settings. Shaded regions indicate the elements analyzed at the respective instrument settings.

the broadest range of natural sample matrices in the study materials. This approach was followed when selecting reference materials from the Woodford, Smithwick, and Eagle Ford Formations (Table 1). Slabbed, clean drill cores containing representative sub-lithologies of these three formations were initially scanned by ED-XRF and inspected in order to determine sample intervals with the broadest range in major and trace element concentrations. Specifically, this was determined by evaluating the elemental peak height within the raw spectra, and selecting samples possessing the full range of low, high, and intermediate peak heights for each element. Because of the range in lithologies and sub-lithologies often found within a given mudrock sequence, it is suggested that a group of no less than ten samples from a given formation should be selected for the purpose of making in-house reference materials. Furthermore, a group of 20–30 reference materials from the same core or a suite of cores possessing similar lithologies is most favorable, especially when many elemental calibrations and a broad range in elemental concentrations are required.

It should be noted that the suite of international standards and reference materials that is readily available to geochemists is not sufficiently diverse for the purposes of properly calibrating the full range of elemental concentrations in most mudrock studies. This is observed in Table 1, wherein the group of five international standards only contains the maximum concentration for one major element (Fe), and none of the minimum elemental concentrations for the entire suite. Whereas, for example, the in-house reference group developed from the Woodford Formation contains nine of the maximum (Mg, Si, Mn, V, Ni, Cu, Zn, U, Mo) and ten of the minimum (Al, P, Ca, Ti, Mn, Th, Sr, Y, Zr, Nb) elemental concentrations for the entire reference suite. Moreover, the Eagle Ford group possesses two of the maximum (Ca and Nb), and ten of the minimum (Mg, Si, K, Fe, Ba, Cr, Ni, Cu, Zn, Rb) elemental concentrations. In essence, the Woodford group covers the silicate-rich, carbonate-poor ranges in elemental concentrations, and expands the upward range of many of the redox-sensitive trace elements (RSTEs), a critical requirement for paleoredox studies. The Eagle Ford group covers the carbonate-rich, silicate-poor ranges in elemental concentrations, and spans most of the compositional range of many of the RSTEs. The group of in-house Smithwick reference materials underpins the analysis of clay-rich samples, as it possesses the greatest range in Al concentrations (12.07%).

Table 2
Corrections used for low-energy and high-energy ED-XRF calibrations.

Element, peak energy	Slope corrections	Background corrections	Number of standard values omitted from calibration[a]
Mg, Ka1	Al, Si, S, Ca, Rh	Mg	0
Al, Ka1	Si, P, Ca, Fe	Al, Rh	3
Si, Ka1	Al, P, Ca, Fe, Rh	Si	0
P, Ka1	Si, P, S, Ca, Fe	P, Rh	0
S, Ka1	Al, Ca, Fe, Rh	S	0
K, Ka1	Ca, Fe	K, Rh	0
Ca, Ka1	Mg, Si, P, Ca, Fe, Rh	K, Ca	0
Ba, La1	K, Ba, Ti, V, Rh	Ca, Ba, Ti	6
Ti, Ka1	Al, Ca, V, Fe, Rh	Ba, Ti	0
V, Ka1	Si, Ba, Ti, V, Rh	V	0
Cr, Ka1	Ca, Mn, Fe, Rh	V, Cr	0
Mn, Ka1	Al, Ti, Rh	Cr, Mn, Fe	12[b]
Fe, Ka1	Ca, Mn, Rh	Fe	0
Ni, Ka1	Ba, Fe, Zn, Rh	Ni	0
Cu, Ka1	Rh	Ni, Cu	3
Zn, Ka1	Cu, Rh	Zn	3
Th, La1	Rh	Th	0
Rb, Ka1	Ca, Th, Rh	Rb, U	5
U, La1	Rh	Rb, U, Sr	20[b]
Sr, Ka1	Ca, Mn, Rb, Sr, Rh	U, Sr	5
Y, Ka1	Th, Rh	Rb, Y	4
Zr, Ka1	Y, Zr, Rh	Sr, Zr	4
Nb, Ka1	Rh	Y, Zr, Nb, Mo	3
Mo, Ka1	Ti	Zr, Nb, Mo	70[b]

[a] Because each standard was analyzed in triplicate, every three values generally represents one standard omission. For example, the three values omitted from the Al calibration are from one reference.
[b] The high number of omissions is largely due to accepted (reference) values that are below the detection limit (i.e., zero values).

4. Results

Linear best-fit calibration curves for major and trace elements are shown in Fig. 2A–X, along with their corresponding slopes and y-intercepts. As a test of calibration validity, and an estimation of error, two reference materials were chosen for further investigation. Seven individual pressed pellets were made from the South African black shale standard, SARM-41, and an equal number were generated for an in-house Woodford Formation shale reference, RTC-W-220, which contains elevated concentrations of RSTEs and other trace elements. An evaluation of their calculated values using the low- and high-energy calibrations, compared to their accepted (reference) values is tabulated in Table 3. Furthermore, the reproducibility of the measurement is reflected in the standard deviation, both between and within pellets of the same reference material. Also listed is the limit of determination of a method (LDM) for each element, for their respective reference materials. The LDM, as calculated according to Rousseau (2001), represents the lowest concentration of an element in a specific sample that can be reliably quantified under a given set of analytical conditions with a 95.4% confidence level. While it does not reflect on the accuracy of a measurement, the

LDM nonetheless provides an estimate of the analytical threshold for samples with similar elemental concentrations.

5. Discussion

5.1. Evaluation of elemental calibrations

Most of the major element calibration curves plotted in Fig. 2A–J possess slopes near unity, y-intercepts near zero, and tight data point clustering about the calibration line. The exceptions are phosphorus and sulfur (Fig. 2D and E). Quantitative phosphorus analyses are hampered by the phosphorus energy peak proximity to that of silicon, and its small peak size relative to that of silicon (Fig. 1A). Quantitative analysis of sulfur is hampered by peak energy proximity to that of rhodium (generated from the x-ray tube), and potentially other matrix-specific conditions. Incidentally, analysis of sulfur by WD-XRF has traditionally been problematic (Gazulla et al., 2009), and it is best analyzed through a combustion-infrared analysis technique (e.g., LECO; Dean and Arthur, 1989). High-quality phosphorus analyses are typically made using WD-XRF. Furthermore, while manganese possesses a usable calibration curve (Fig. 2I), the overwhelming majority of the reference materials have Mn concentrations less than 20% of the full range of references; thus, a broader range of reference materials is needed to define and refine the calibration curve.

The majority of the trace element calibration curves observed in Fig. 2K–X possess slopes near unity, y-intercepts near but above the origin, and strong clustering about the calibration line. Eight of the fourteen trace element calibrations possess slopes between 0.93 and unity, and four possess slopes between 0.83 and 0.93. Slopes for Cr and Nb are greater than 0.77, suggesting an, as yet unknown, instrumental or calibration routine bias. Calibrations for Ba, V, Ni, and Cu (Fig. 2K, L, N, O) require more high-concentration standards to support the curve. The LDMs for these elements and Zn (Fig. 2P) are elevated relative to other analytical techniques. The cause of the high LDMs is unclear; however, it is probably not the pellet-making process, because high LDMs would be expected in all the elements if that were the case. High LDMs may suggest that the mineral phase(s) responsible for such elements is not as easily homogenized relative to other phases. Furthermore, the Cr analysis (Fig. 2M) possesses a higher analytical threshold, below which its calibration appears to

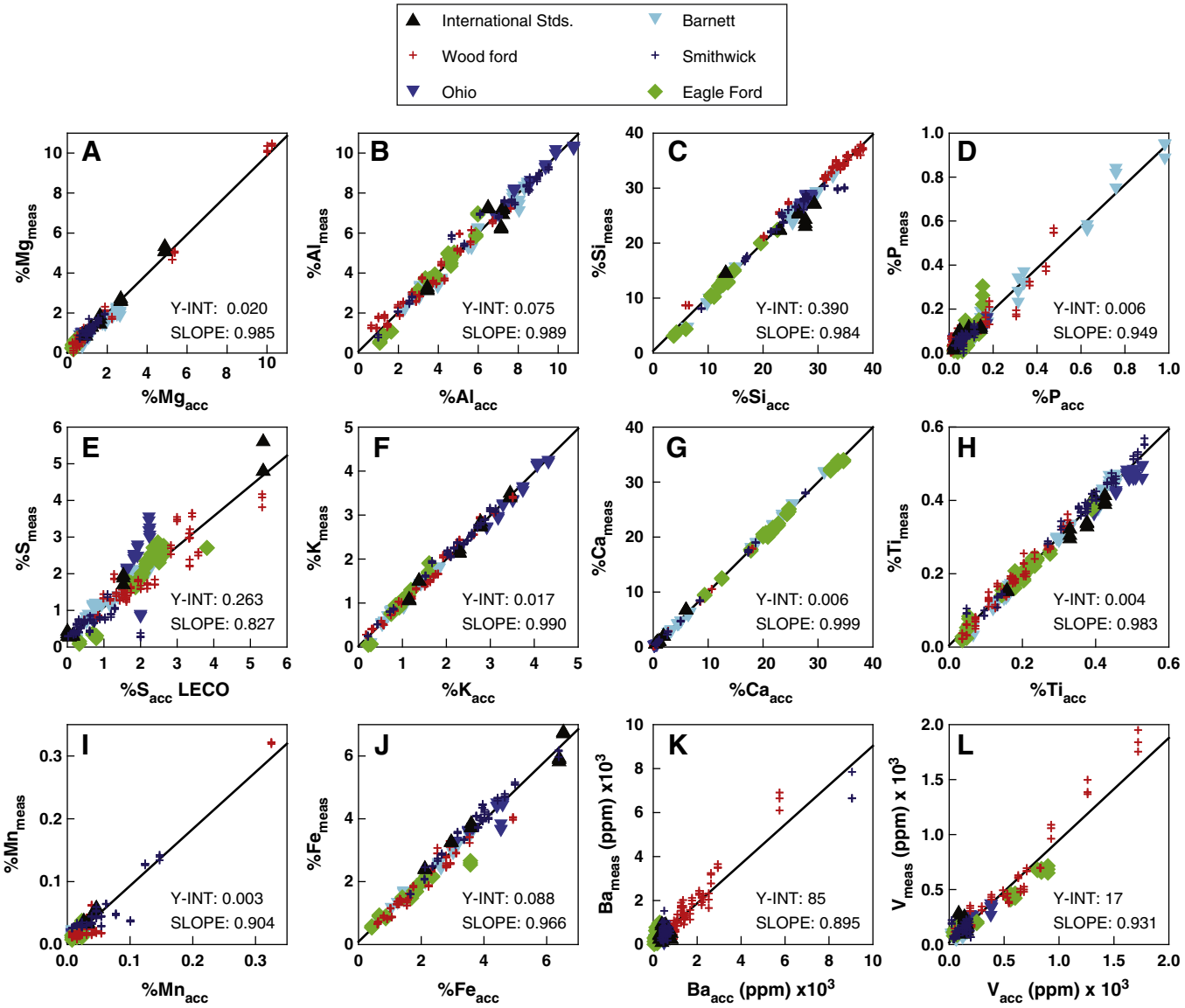

Fig. 2. Accepted (acc) versus measured (meas) values for elements analyzed by WD-XRF or ICP-MS/ICP-OES and ED-XRF, respectively. Measured values were determined using the Bruker AXS *S1CAL Process* software, with reference values, raw spectra, and inter-element corrections as inputs (Table 2). The legend denotes the reference material suite from which each data point is derived. Note: the results of three analyses are plotted for each reference.

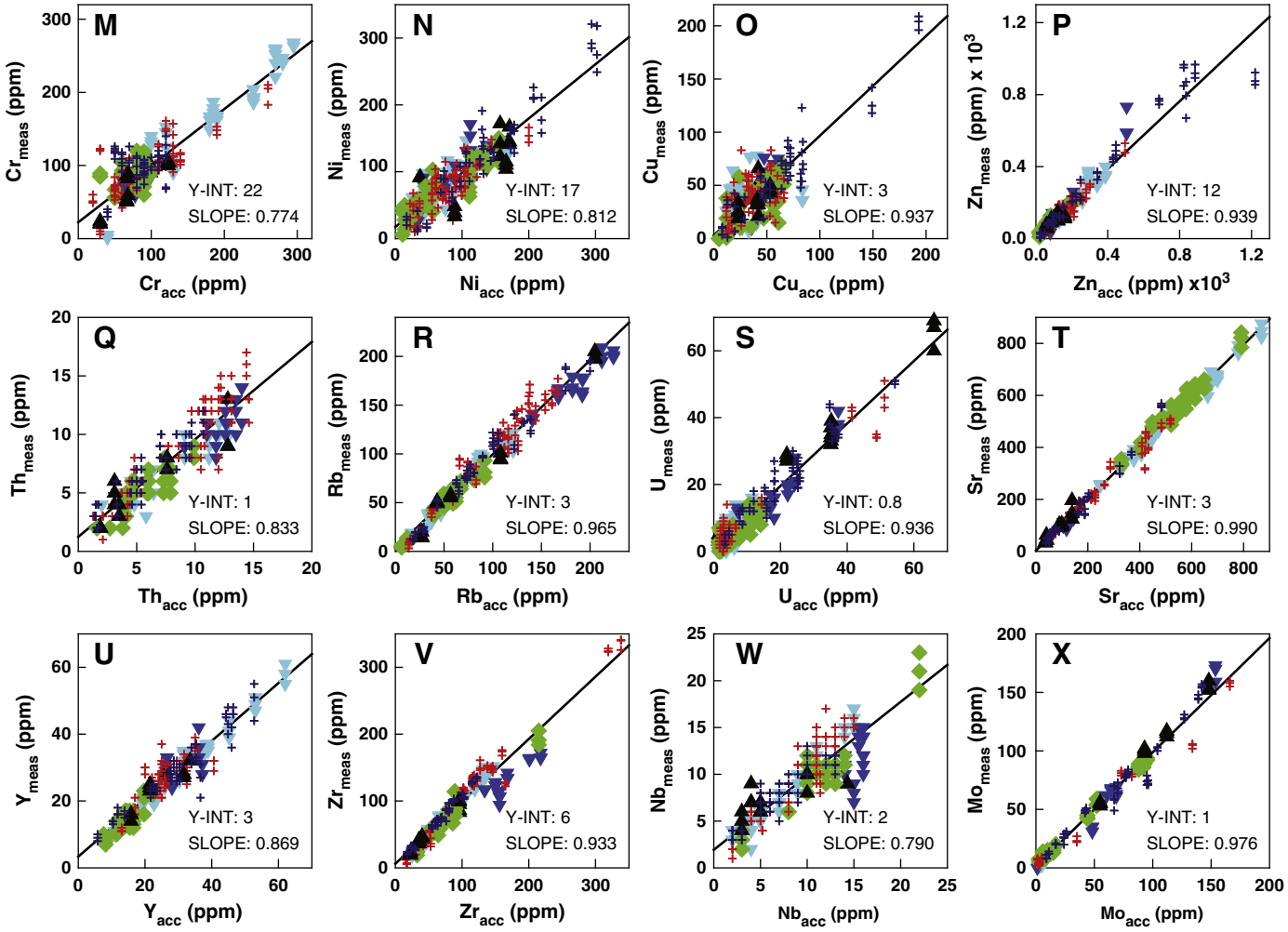

Fig. 2 (*continued*).

Table 3
Accepted versus measured elemental concentrations, inter-pellet standard deviations, intra-pellet standard deviation, and limits of determination of a method for one internationally accepted standard (SARM-41), and one in-house reference material (RTC-W-220) prepared using pulverized sample from the Mississippian-age Woodford Formation.

Element	SARM-41					RTC-W-220 (Woodford Fm.)				
	Accepted value[a]	Measured value[b]	$\sigma_{7pellets}$[c]	$\sigma_{1pellet}$[d]	LDM[e]	Accepted value[a]	Measured value[b]	$\sigma_{7pellets}$[c]	$\sigma_{1pellet}$[d]	LDM[e]
Mg (%)	4.9	5.0	0.17	0.20	0.33	0.67	0.80	0.09	0.17	0.17
Al (%)	7.14	5.89	0.14	0.10	0.28	4.96	5.39	0.14	0.05	0.28
Si (%)	26.5	24.0	0.2	0.2	0.5	32.6	33.7	0.2	0.2	0.5
P (%)	0.02	0.02	0.02	0.01	0.03	0.07	0.05	0.03	0.03	0.07
S (%)	0.15	0.19	0.02	0.01	0.04	3.34	2.18	0.10	0.04	0.20
K (%)	1.15	1.02	0.02	0.02	0.04	2.07	2.31	0.09	0.04	0.18
Ca (%)	1.07	0.99	0.03	0.01	0.06	0.13	0.23	0.03	0.00	0.06
Ti (%)	0.33	0.29	0.01	0.02	0.02	0.23	0.27	0.02	0.01	0.04
Mn (%)	0.046	0.056	0.003	0.002	0.006	0.015	0.012	0.001	0.001	0.002
Fe (%)	2.96	3.20	0.03	0.01	0.06	2.93	2.55	0.06	0.02	0.12
Ba (ppm)	820	802	214	147	428	2090	1884	376	83	753
V (ppm)	139	167	41	44	82	928	1114	68	66	137
Cr (ppm)	123	106	16	9	32	110	98	13	9	26
Ni (ppm)	122	79	17	8	34	130	153	26	20	52
Cu (ppm)	53	65	24	14	48	83	147	20	16	40
Zn (ppm)	76	67	7	11	14	823	844	96	30	191
Th (ppm)	12	7	1	1	2	8.4	9	1	2	2
Rb (ppm)	59	45	3	3	6	122	123	12	4	25
U (ppm)	2	3	2	3	4	18.1	17	6	4	11
Sr (ppm)	54	47	2	1	4	75.5	87	5	4	10
Y (ppm)	17	17	1	1	3	35.4	34	3	2	5
Zr (ppm)	146	130	5	4	11	80.3	95	7	2	13

Table 3 (*continued*)

Element	SARM-41					RTC-W-220 (Woodford Fm.)				
	Accepted value[a]	Measured value[b]	$\sigma_{7pellets}$[c]	$\sigma_{1pellet}$[d]	LDM[e]	Accepted value[a]	Measured value[b]	$\sigma_{7pellets}$[c]	$\sigma_{1pellet}$[d]	LDM[e]
Nb (ppm)	8	5	1	1	2	9	9	1	1	2
Mo (ppm)	5	8	1	1	2	79	83	4	4	9

[a] SARM-41 accepted values taken from certificate of authentication and from literature (Govindaraju, 1994). For RTC-W-220, values for major elements are from lithium borate-fused disk analysis by WD-XRF at SGS; values for trace elements (ppm) from sodium peroxide fusion dissolution and analysis by ICP-MS and ICP-OES. Values for %S determined by LECO combustion/infrared analysis.
[b] Average calibrated handheld ED-XRF-measured values from 7 identically prepared pellets.
[c] Standard deviation from measuring 7 identically prepared pellets.
[d] Standard deviation from analyzing 1 of the pressed pellets 7 times.
[e] Limit of Determination of a Method (LDM) calculated according to Rousseau (2001).

have greater error. Specifically, the spread in the Cr calibration below ~70 ppm is greater than at higher concentrations. This does not appear to be the case with other elements (e.g., Rb, Sr, U, Mo).

As a test of calibrated data fidelity with respect to a traditionally more accepted analytical technique, Fig. 3A–X show the Barnett Formation chemostratigraphies of the twenty-four calibrated elements

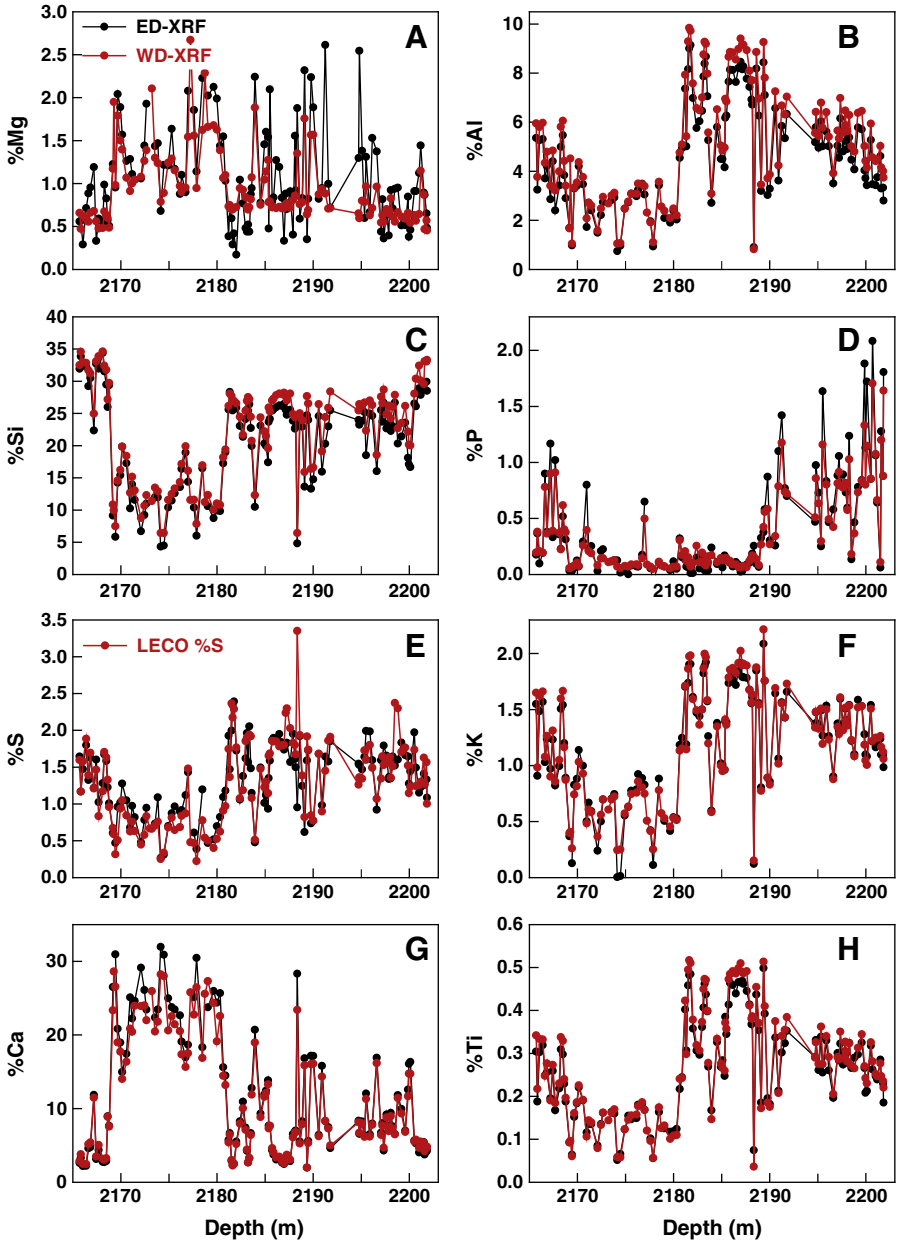

Fig. 3. Comparison of chemostratigraphic data generated using a Bruker TRACER III-V ED-XRF (black) and a Bruker S4 WD-XRF (red). Pressed pellets originally analyzed by WD-XRF provide remarkably similar ED-XRF-derived results for most elements. Pellets were analyzed by ED-XRF for 180 s at both low- and high-energy. The significant number of missing ED-XRF values for Ba indicates where the calibration returned a negative number (K).

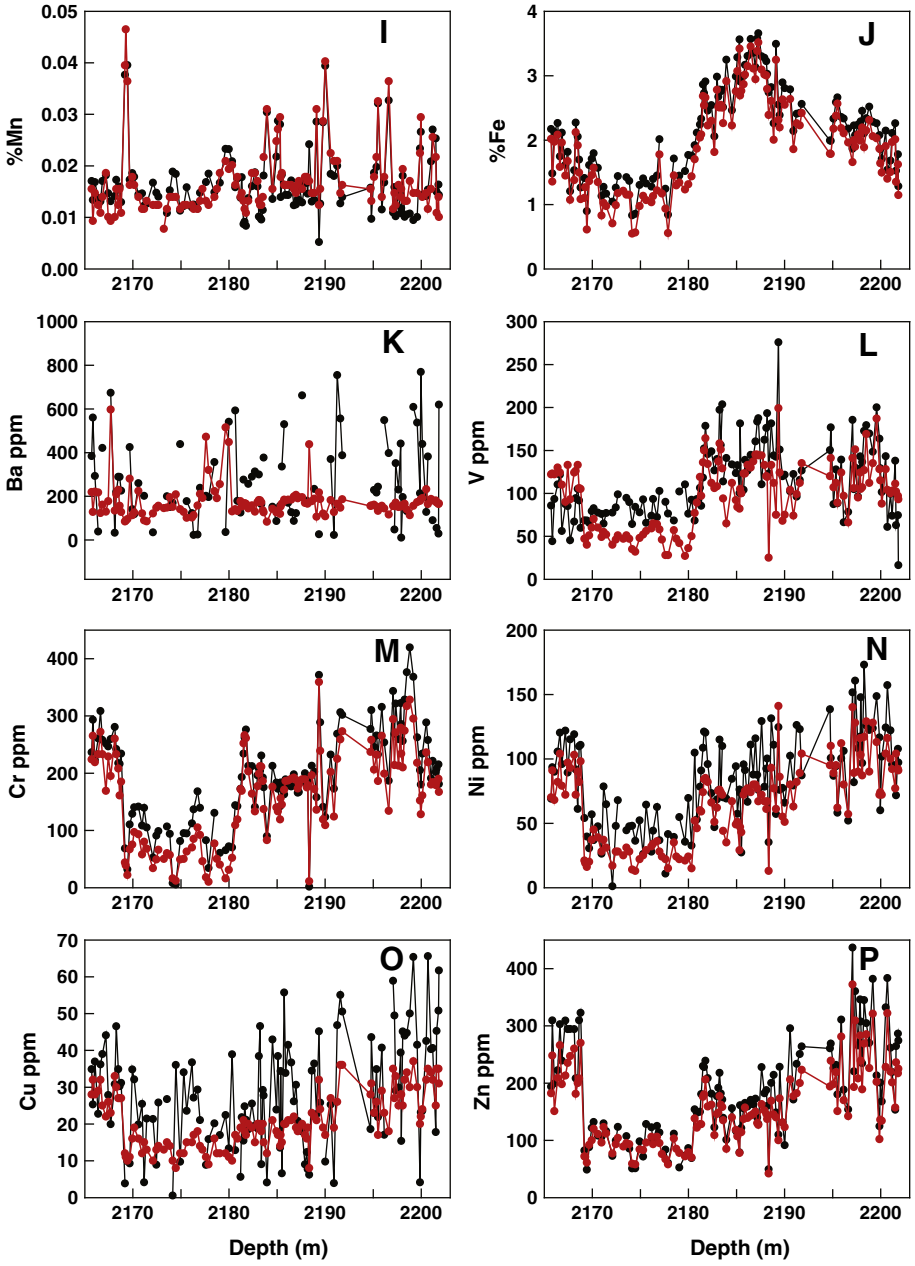

Fig. 3 (*continued*).

in the 1-Blakely drill core from Wise County, Texas, USA (Loucks and Ruppel, 2007; Rowe et al., 2008), with the calibrated output from both the ED-XRF and the Bruker AXS S4 Pioneer WD-XRF instrument housed at the Kentucky Geological Survey. The S4 Pioneer was calibrated with international standards and with the Ohio Shale reference materials listed in Table 1. Analyses for each instrument were undertaken using pressed pellets of the Barnett samples, prepared in the same manner as the standards and reference materials (Section 2). Specifically, these analyses are plotted in Figs. 3, 4, and 5.

With few exceptions, across a broad range of elemental composition and a significant difference in the number and elemental range of reference materials, Fig. 3A–J demonstrates that the calibrated major element output from the ED-XRF is not only correlated with, but possesses a near one-to-one relationship with the WD-XRF results. Significant divergences between the two datasets are observed in the Mg and P chemostratigraphies (Fig. 3A and D), and less significant divergences are observed in Al, Si, Ca, and Fe (figures B, C, G, J). In each of these cases, the divergences between the black (ED-XRF) and red (WD-XRF) chemostratigraphic results tend to be systematic. For example, samples with elevated concentrations of Ca tend to have higher %Ca values using the ED-XRF calibration versus using the WD-XRF calibration (Fig. 3G). The same is true for Mg, P, and Fe, and is largely opposite for Si and P. It is hypothesized that these divergences are, in large part, reflecting the difference in the number of standards used (and thus, their concentrations) to calibrate the WD-XRF (<30) versus the ninety references used to calibrate the ED-XRF.

While a similar observation regarding systematic (or quasi-systematic) offset can be made when evaluating the trace element chemostratigraphies (e.g., Cr, Ni, Zn, Rb, U, Y, Fig. 3M, N, P, R, S, U), some element concentration ranges tend to be expanded with the ED-XRF calibration relative to the WD-XRF calibration (e.g., the high values are higher, and the low values are lower with the ED-XRF calibration). This appears to be the case for Cu and Th (Fig. 3O, Q), to a varying degree for V (Fig. 3L), and perhaps for Ba (Fig. 3K), although both ED-XRF and WD-XRF calibrations for Ba potentially suffer from inter-elemental influences (e.g. Ti). Again, it is suggested that the

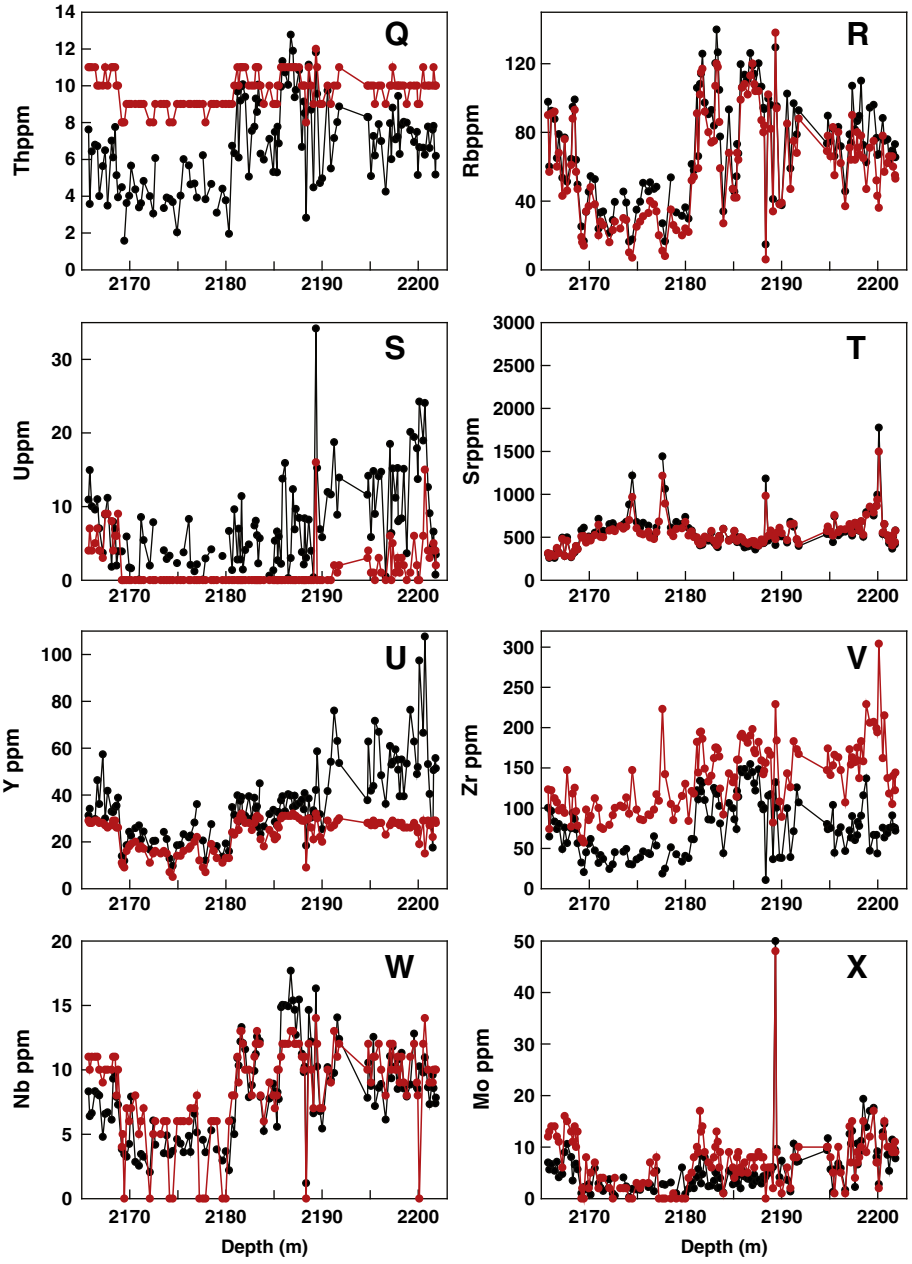

Fig. 3 (*continued*).

divergences observed in the ED-XRF and WD-XRF chemostratigraphies are largely the results of differences in the range of calibration standards between the two different instruments. Nonetheless, the absolute concentrations derived from the different techniques are highly correlated, a verification for the utilization of ED-XRF for research-grade analysis of clean, flat mudrock surfaces. It should also be noted that preliminary comparison work between Bruker TRACER III–V units suggests that equivalent results are obtained, as long as the instrument settings are optimized.

5.2. Applications to chemostratigraphy and paleo-redox studies

In addition to defining the chemostratigraphic shifts in a mudrock sequence (Fig. 3A–X), elemental concentrations and ratios of concentrations can be utilized to define stratigraphic shifts in mineralogy, and in some cases, large-scale changes in water mass conditions during deposition (e.g., paleo-redox). A Ca–Al–Si ternary diagram (Brumsack, 1989) demonstrates the fidelity of the ED-XRF results from the 1-Blakely core (Barnett Formation), with respect to the WD-XRF results (Fig. 4). The ternary indicates that Barnett mudrocks are mildly silica-rich, relative to the average shale (Wedepohl, 1971). Furthermore, the silica and aluminosilicate components are diluted by the presence of $CaCO_3$ in many of the samples, evidenced by the trend toward the 2xCaO end-member. Most mudrock sequences possess high abundances of calcite, clay, and/or quartz, thereby making this type of diagram useful in defining their bulk mineralogical variations.

Elemental variations in Fe, S, Si, Al, and Mo, derived from ED-XRF and WD-XRF analyses of the 1-Blakely core samples are also compared in Fig. 5A–C. Fig. 5A reveals the Fe–S associations, which, in organic-rich mudrock sequences, are generally dominated by the mineral pyrite (Dean and Arthur, 1989; Rimmer, 2004), and may also provide information on the abundance of other phases that partition Fe (e.g., siderite, dolomite, ankerite, vivianite, and clays), and S (gypsum/anhydrite, barite, celestite). Specifically, Fig. 5A indicates that all samples fall to the right of the pyrite line, and many of the samples define a sub-grouping that is sub-parallel to the pyrite line,

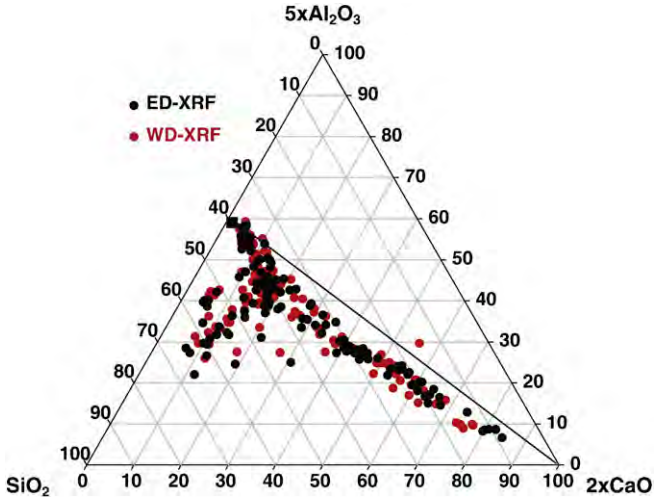

Fig. 4. A ternary plot demonstrating relative variations in CaO, Al_2O_3, and SiO_2, assumed to reflect bulk mineralogical changes in calcite, clay, and quartz, respectively (Brumsack, 1989). Black filled circles indicate data generated by handheld ED-XRF, and red filled circles indicate data generated by WD-XRF. The black square denotes "average shale" (Wedepohl, 1971; Brumsack, 1989), and the black line demonstrates the trajectory along which low-$CaCO_3$ average shale would be diluted by calcite.

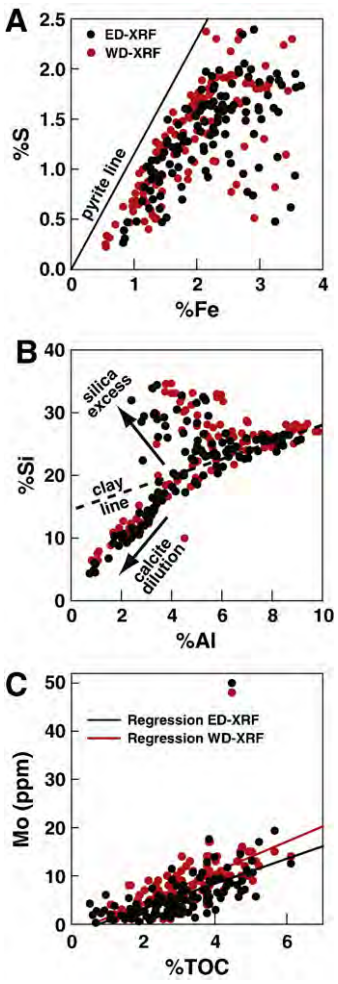

Fig. 5. Geochemical relationships in the Barnett Shale, 1-Blakely core, Wise, County, TX, USA. A) S–Fe relationships demonstrated using ED-XRF (black) and WD-XRF results (red). B) Si-Al relationships demonstrating partitioning of Si and Al into clay and quartz, and the dilution of the aluminosilicates by calcite. Sub-groupings are denoted by Si-excess, calcite-diluted samples, and samples that fall along a well-defined clay line. C) Mo-TOC relationships, demonstrating very low degrees of Mo enrichment, relative to the amount of TOC. Red (black) lines reflect the best-fit regression through the ED-XRF (WD-XRF) results, respectively. In all cases, the ED-XRF results are highly consistent with results generated using the traditional WD-XRF technique. A description of the analytical techniques used for the generation of LECO-%S and TOC can be found in Rowe et al. (2008).

suggesting that pyrite is an important constituent in the Barnett Formation, but that a significant Fe-excess must be associated with non-sulfur phases. This is confirmed by x-ray diffraction work on the samples (Rowe et al., 2008). The ED-XRF calibration for S is not as robust as it is for elements like Fe (Section 4; Fig. 2E and J), and in other organic-rich mudrock sequences, despite S–Fe linkages confirmed by x-ray diffraction, the ED-XRF sulfur analyses do not demonstrate the intimate linkage between S and Fe. It is hypothesized that a sample matrix effect is responsible for the weakness in S analysis, and further analytical development focused on ED-XRF analysis of sulfur is required.

The Si–Al associations in the Barnett (Fig. 5B) suggest that, while there is a well-defined linear relationship between the two elements indicative of their co-occurrence in clays, there is also a silica-excess (above the clay line) that is interpreted to be either biogenic or detrital quartz. Samples defining strong linearity between Al and Si at lower concentrations for both elements are believed to indicate dilution by calcite (Rowe et al., 2008). Interpretation of Fig. 5B essentially confirms what can be determined from analysis of Fig. 4.

Molybdenum-TOC associations are used to assess deep-basin water mass restriction and overall anoxia (Algeo and Lyons, 2006). It has previously been demonstrated, using the WD-XRF results from the 1-Blakely core samples, that the Mo-TOC relationship indicates severe water mass restriction during Barnett deposition, possibly indicative of water mass residence times of several tens of thousands of years (Rowe et al., 2008). ED-XRF and WD-XRF results for Mo versus the sample %TOC are plotted in Fig. 5C, and, as in Fig. 3X, it can be observed that Mo concentrations measured using both x-ray techniques strongly track each other. The slopes and intercepts of the regression lines through each dataset are very similar, indicating that the ED-XRF results essentially support the same conclusion as that derived using the WD-XRF results.

6. Conclusions

Rapid, real-time, quantitative mudrock chemostratigraphies can be generated using a research-grade, handheld ED-XRF unit that has been calibrated with a diverse suite of mudrock reference materials. Preparation, analysis, and calibration strategy are demonstrated and defined in detail, and the sample reproducibility, limits of determination of a method, and inter-instrument comparison with WD-XRF yield results that support the use of the instrument for quantitative analysis of fine-grained sedimentary rocks. While the method is robust for many elements, further development in analysis conditions (changing voltage, current, beam filtering) and post-analysis processing (inter-element and background corrections) is required. The elements requiring the most focus for future work are P, S, Ba, and Cr. Implementation of the handheld ED-XRF into traditional lithostratigraphic and biostratigraphic studies can provide unique insights into the paleoenvironmental conditions during and after deposition. At the very least, the ED-XRF provides a robust "first look" at drill core chemostratigraphy, and can be employed to refine the sampling strategy for more detailed, labor-intensive chemostratigraphic and isotopic analysis.

Acknowledgments

The comments from anonymous reviewers are deeply appreciated. We are thankful for discussions with and critical support from Henry

Francis, Andrea Connor, Jason Backus, Patrick Gooding, Ray Daniel, and James Cobb (Kentucky Geological Survey), Sue Rimmer (Southern Illinois University), Barry Maynard (University of Cincinnati), and Stephen Ruppel and industry associates of the Mudrock Systems Research Laboratory (Texas Bureau of Economic Geology). Furthermore, we are indebted to James Donnelly, Nathan Ivicic, Kenneth Edwards, and Josh Lambert (Core Research Center, Texas Bureau of Economic Geology). We also thank Scott Delorme, Bonnie White, Bernadette LeBoeuf, Mohibur Rahman, and I-Ching Lee (SGS Minerals Services, Canada). We especially thank Dr. Bruce Kaiser and Bruker AXS, Inc., for their discussions, support, and continued assistance with instrumentation access and development. We also thank the University of Texas at Arlington, Geological Society of America, American Association of Petroleum Geology, and Gulf Coast Association of Geological Societies for supporting the thesis work of Niki Hughes, and the Fort Worth Geological Society and Pioneer Natural Resources Company for supporting the thesis work of Krystin Robinson. This study was supported by US National Science Foundation Instrumentation and Facilities Grant #0949384 to HDR.

References

Algeo, T.J., Lyons, T.W., 2006. Mo–total organic carbon covariation in modern anoxic marine environments: implications for analysis of paleoredox and paleohydrographic conditions. Paleoceanography 21, PA1016, doi:10.1029/2004PA001112.

Algeo, T.J., Maynard, J.B., 2008. Trace-metal covariation as a guide to water-mass conditions in ancient anoxic marine environments. Geosphere 4, 872–887.

Brumsack, H.J., 1989. Geochemistry of recent TOC-rich sediments from the Gulf of California and the Black Sea. Geologische Rundschau 78, 851–882.

Dean, W.E., Arthur, M.A., 1989. Iron-sulfur-carbon relationships in organic-carbon-rich sequences I: Cretaceous Western Interior Seaway. American Journal of Science 289, 708–743.

Fitton, G., 1997. X-ray fluorescence spectrometery. In: Gill, Robin (Ed.), Modern Analytical Geochemistry. Addison Wesley Longman. 329 pp.

Gazulla, M.F., Gomez, M.P., Oduña, M., Rodrigo, M., 2009. New methodology for sulfur analysis in geological samples by WD-XRF spectrometry. X-Ray Spectrometry 38, 3–8.

Govindaraju, K., 1994. 1994 Compilation of working values and sample description for 383 geostandards. Geostandards Newsletter 18 (S1), 1–158.

Haug, G.H., Hughen, K.A., Sigman, D.M., Peterson, L.C., Röhl, U., 2001. Southward migration of the intertropical convergence zone through the holocene. Science 293, 1304–1308.

Jansen, J.H.F., Van der Gaast, S.J., Koster, B., Vars, A.J., 1999. CORTEX, a shipboard XRF-scanner for element analyses in split sediment cores. Marine Geology 151, 143–153.

Kujau, A., Nürnberg, D., Zielhofer, C., Bahr, A., Röhl, U., 2010. Mississippi River discharge over the last 560,000 years — indications from x-ray fluorescence core-scanning. Palaeogeography, Palaeoclimatology, Palaeoecology 298, 311–318.

Loucks, R.G., Ruppel, S.C., 2007. Mississippian Barnett Shale: lithofacies and depositional setting of a deep-water shale-gas succession in the Fort Worth Basin, Texas. AAPG Bulletin 91, 579–601.

Norrish, K., Hutton, J.T., 1969. An accurate x-ray spectrographic method for the analysis of a wide range of geological samples. Geochimica et Cosmochimica Acta 33, 431–453.

Potts, P.J., Webb, P.C., 1992. X-ray fluorescence spectrometry. Journal of Geochemical Exploration 44, 251–296.

Richter, T.O., Van der Gaast, S., Koster, B., Vaars, A., Gieles, R., de Stigter, H.C., Haas, H.D., van Weering, T.C.E., 2006. The Avaatech XRF core scanner: technical description and applications to NE Atlantic sediments. Geological Society, London. Special Publication 267, 39–50.

Rimmer, S.M., 2004. Geochemical paleoredox indicators in Devonian–Mississippian black shales, Central Appalachian Basin (USA). Chemical Geology 206, 373–391.

Rousseau, R.M., 2001. Detection limit and estimate of uncertainty of analytical XRF results. The Rigaku Journal 18, 33–47.

Rowe, H.D., Loucks, R.G., Ruppel, S.C., Rimmer, S., 2008. Mississippian Barnett Formation, Fort Worth Basin, Texas: bulk geochemical inferences and Mo-TOC constraints on the severity of hydrographic restriction. Chemical Geology 257, 16–25.

Tertian, R., Claisse, F., 1994. Principles of quantitative x-ray fluorescence analysis. Wiley, Chichester. 385 pp.

Tjallingii, R., Röhl, U., Kölling, M., Bickert, T., 2007. Influence of the water content on x-ray fluorescence core-scanning measurements in soft marine sediments. Geochemistry, Geophysics, Geosystems 8 (2) 12 pp.

Tung, J.W.T., 2004. Determination of metal components in marine sediments using energy-dispersive x-ray fluorescence (ED-XRF) spectrometry. Annali di Chimica 94, 837–846.

Wedepohl, K.H., 1971. Environmental influences on the chemical composition of shales and clays. In: Ahrens, L.H., Press, F., Runcorn, S.K., Urey, H.C. (Eds.), Physics and Chemistry of the Earth, vol. 8. Pergamon, Oxford, pp. 305–333.